An energy-momentum scheme for frictional contact in flexible multibody dynamics.

Marlon Franke, Christian Hesch, Peter Betsch

Chair of Computational Mechanics
University of Siegen
Paul-Bonatz-Str. 9-11, 57068 Siegen, Germany
[marlon.franke, christian.hesch, peter.betsch]@uni-siegen.de

ABSTRACT

The present contribution deals with the frictional contact of flexible bodies. In particular we investigate the time integration of dynamic contact problems with large deformations. The overall aim is to compare standard with recently developed integrators. To this end we propose an energy and momentum consistent integrator which exhibits superior numerical stability.

1 INTRODUCTION

The aim of our work is to develop stable integrators for transient large deformation contact problems (see e.g. Reference [13]). Using the widely-used node-to-surface method, where we enforce the constraints by Lagrange multipliers, we obtain a unified system of index-3 differential-algebraic equations (DAE). Within this common framework we are able to incorporate structural elements such as shells, beams, continua as well as rigid bodies for which we use a rotationless formulation (see References [12, 11]). For the underlying DAE's even second order implicit integrators like e.g. the midpoint rule or the Newmark method fail to deal in a consistent way with various physical properties of the system, resulting in an unstable numerical behavior of the system. To avoid this disadvantage we apply an energy-momentum scheme, which has already been investigated in the context of nonlinear elastodynamics (see References [2, 4]). In the context of contact mechanics similar consistent integrators have been applied previously (see References [1, 10]), violating the non-penetration condition. The present work builds on the previous works (see References [3, 6]).

2 Continuum and contact mechanics

In order to simplify the notation for frictional multibody contact problems we restrict our consideration on a two body contact problem (see Figure 1). Therefore the bodies are depicted in the reference configuration $\mathcal{B}_0^{(i)} \subset \mathbb{R}^3, i \in [1,2]$ and in the current configuration $\mathcal{B}_t^{(i)} \subset \mathbb{R}^3, i \in [1,2]$, respectively. The material boundaries of the bodies can be decomposed into the Neumann boundary Γ_n, the Dirichlet boundary Γ_d and in the contact surface Γ_c. The spatial counterparts of the boundaries are denoted with γ_n, γ_d and γ_c. In this connection we presume that the boundaries satisfy:

$$\partial\mathcal{B}_0^{(i)} = \Gamma_n^{(i)} \cup \Gamma_c^{(i)} \cup \Gamma_d^{(i)} \quad \text{and} \quad \Gamma_n^{(i)} \cap \Gamma_c^{(i)} = \Gamma_n^{(i)} \cap \Gamma_d^{(i)} = \Gamma_c^{(i)} \cap \Gamma_d^{(i)} = \emptyset \tag{1}$$

Any material configuration of the bodies can be addressed via $\boldsymbol{X}^{(i)}$ and we obtain the spatial counterpart using the mapping $\boldsymbol{\varphi}^{(i)}\left(\boldsymbol{X}^{(i)}\right)$. We assume that the bodies come in contact within the considered time interval $t \in \mathcal{I} := [0,T]$. The balance of linear momentum with respect to the reference configuration reads

$$\rho_0^{(i)} \ddot{\boldsymbol{\varphi}}^{(i)} = \text{DIV}(\boldsymbol{P}^{(i)}) + \boldsymbol{B}^{(i)} \tag{2}$$

where $\boldsymbol{B}^{(i)}$ denotes the body force per reference volume, $\rho_0^{(i)} \ddot{\boldsymbol{\varphi}}^{(i)}$ denotes the inertia force term corresponding to the i-th body $\mathcal{B}_0^{(i)}$ using the reference density $\rho_0^{(i)}$ and $\boldsymbol{P}$ denotes the first Piola-Kirchhoff stress tensor, which depends on the considered constitutive law described via the strain energy function $W^{(i)}$. For the initial/boundary value problem (see Equation (2)) we have to take the boundary and the initial conditions
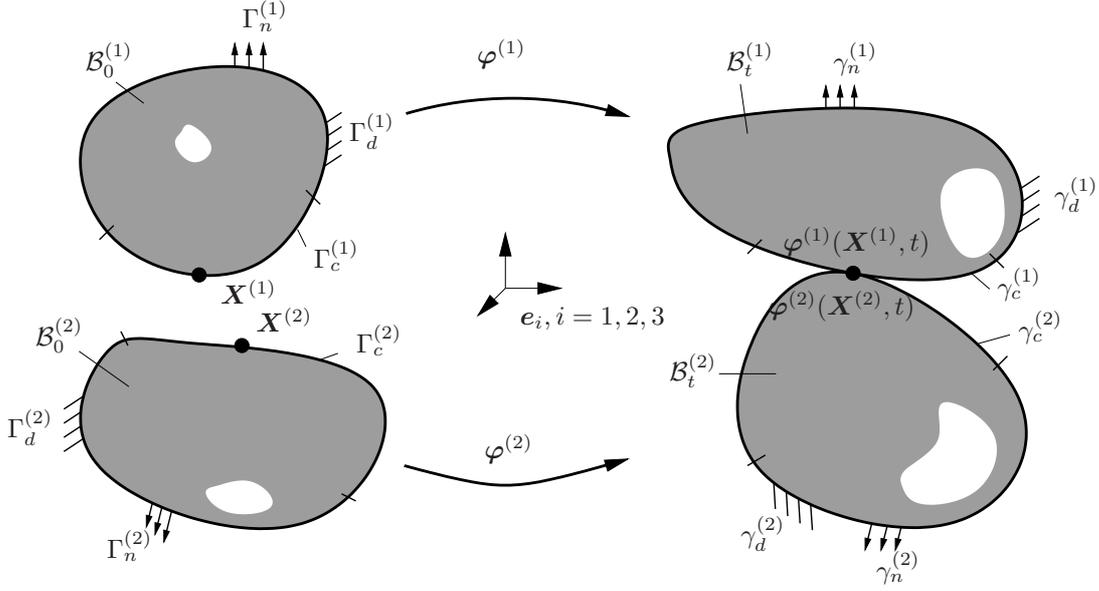
Figure 1. Configurations of two body contact ($\mathcal{B}_0^{(i)}$: bodies in the reference configuration, $\mathcal{B}_t^{(i)}$: bodies in the current configuration)

into account. Hence the boundary conditions are given as

$$\boldsymbol{\varphi}^{(i)} = \bar{\boldsymbol{X}}^{(i)} \quad \text{in } \Gamma_d^{(i)} \, \forall \, t \in \mathcal{I} \tag{3}$$

$$\boldsymbol{T}^{(i)} = \boldsymbol{P}^{(i)} \, \boldsymbol{N}^{(i)} = \bar{\boldsymbol{T}}^{(i)} \quad \text{in } \Gamma_n^{(i)} \, \forall \, t \in \mathcal{I} \tag{4}$$

where $\boldsymbol{T}^{(i)}$ denotes the Piola traction vector and $\boldsymbol{N}^{(i)}$ denotes the unit outward normal of $\Gamma_n^{(i)}$. $\bar{\boldsymbol{X}}^{(i)}$ and $\bar{\boldsymbol{T}}^{(i)}$ denote the prescribed displacement and traction respectively. At last we provide the initial conditions

$$\boldsymbol{\varphi}^{(i)}(t=0) = \boldsymbol{X}_0^{(i)} \quad \text{in } \mathcal{B}_0^{(i)} \tag{5}$$

$$\dot{\boldsymbol{\varphi}}^{(i)}(t=0) = \boldsymbol{V}_0^{(i)} \quad \text{in } \mathcal{B}_0^{(i)} \tag{6}$$

In order to deduce the contribution of each body to the weak form of the boundary value problem we define the solution space

$$\mathcal{V}_s^{(i)} = \{\boldsymbol{\varphi}^{(i)} \in H^1(\mathcal{B}^{(i)}) : \boldsymbol{\varphi}^{(i)} = \bar{\boldsymbol{\varphi}}^{(i)} \text{ on } \Gamma_d^{(i)}\} \tag{7}$$

and the space of test functions

$$\mathcal{V}_t^{(i)} = \{\delta\boldsymbol{\varphi}^{(i)} \in H^1(\mathcal{B}^{(i)}) : \delta\boldsymbol{\varphi}^{(i)} = \boldsymbol{0} \text{ on } \Gamma_d^{(i)}\} \tag{8}$$

where the Sobolev space $H^1(\mathcal{B}^{(i)})$ consists of the spaces of square integrable functions and their first derivatives. The weak form for the problem at hand reads

$$\overbrace{\int_{\mathcal{B}_0^{(i)}} \rho_0^{(i)} \, \ddot{\boldsymbol{\varphi}}^{(i)} \cdot \delta\boldsymbol{\varphi}^{(i)} \, \mathrm{d}V}^{=:G^{(i),dyn}} + \overbrace{\int_{\mathcal{B}_0^{(i)}} \boldsymbol{P}^{(i)} : \mathrm{Grad}(\delta\boldsymbol{\varphi}^{(i)}) \, \mathrm{d}V}^{=:G^{(i),int}}$$

$$= \underbrace{\int_{\mathcal{B}_0^{(i)}} \rho_0^{(i)} \, \bar{\boldsymbol{B}}^{(i)} \cdot \delta\boldsymbol{\varphi}^{(i)} \, \mathrm{d}V + \int_{\Gamma_n^{(i)}} \bar{\boldsymbol{T}}^{(i)} \cdot \delta\boldsymbol{\varphi}^{(i)} \, \mathrm{d}A}_{=:G^{(i),ext}} + \underbrace{\int_{\Gamma_c^{(i)}} \boldsymbol{t}^{(i)} \cdot \delta\boldsymbol{\varphi}^{(i)} \, \mathrm{d}A}_{=:G^{(i),c}} \quad \forall \, \delta\boldsymbol{\varphi}^{(i)} \in \mathcal{V}_t^{(i)} \tag{9}$$

As indicated in Equation (9) we obtain the virtual work for the considered bodies:

$$G\left(\boldsymbol{\varphi}, \delta\boldsymbol{\varphi}\right) = \sum_{i=1}^{2}\left(G^{(i),dyn} + G^{(i),int} - G^{(i),ext} - G^{(i),c}\right) = 0 \tag{10}$$

Additionally we postulate that the local momentum balance on the contact boundary

$$-\boldsymbol{t}^{(2)}\ \mathrm{d}A = \boldsymbol{t}^{(1)}\ \mathrm{d}A \tag{11}$$

holds. Thus, the contact contribution to the virtual work reads

$$G^{c} = \sum_{i}^{2} G^{(i),c} = \int_{\Gamma_{c}^{(1)}} \boldsymbol{t}^{(1)} \cdot \left[\delta\boldsymbol{\varphi}^{(1)} - \delta\boldsymbol{\varphi}^{(2)}\right]\ \mathrm{d}A \tag{12}$$

The fundamental balance principles, namely the balance laws for the linear momentum $\boldsymbol{L}$, the angular momentum $\boldsymbol{J}$ as well as the total energy E of the system should hold during the considered time interval $\mathcal{I}$ as depicted in Table 1, where $\tilde{\boldsymbol{F}}^{(i)}$ denotes the resultant forces, $\tilde{\boldsymbol{M}}^{(i)}$ the resultant momenta and $P^{(i),ext}$ the resultant external power. In case of a conservative problem (e.g. frictionless contact and pure stick contact), the fundamental balance principles are maintained.

Balance principles	
Linear momentum:	$\dot{\boldsymbol{L}} = \sum_{i=1}^{2} \tilde{\boldsymbol{F}}^{(i)}$
Angular momentum:	$\dot{\boldsymbol{J}} = \sum_{i=1}^{2} \tilde{\boldsymbol{M}}^{(i)}$
Energy:	$\dot{E} = \sum_{i=1}^{2}\left(\dot{T}^{(i)} + \dot{V}^{(i)}\right) = \sum_{i=1}^{2} P^{(i),ext}$

Table 1. Balance principles for bodies $\mathcal{B}_{0}^{(i)}$

For detailed derivation of the balance principles like the linear and angular momentum as well as the total energy of the system we refer to Reference [7].

3 Contact description
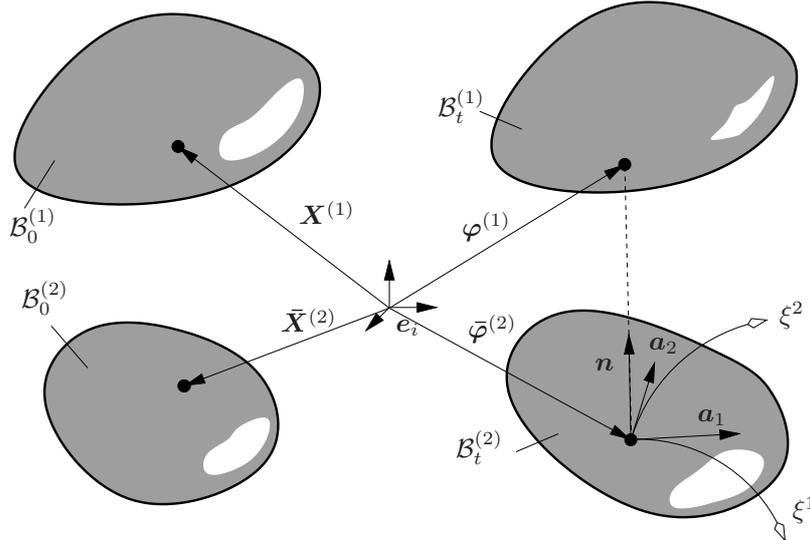
Figure 2. Parametrization of the contact surfaces

For the contact description we use the so-called direct approach (see Reference [9]) but also other descriptions like e.g. the covariant approach (see Reference [8]) are suitable. For further considerations we use the

well-known slave-master concept (see Reference [5]). To this end we determine $\boldsymbol{X}^{(1)} \in \Gamma_c^{(1)}$ and its spatial counterpart $\boldsymbol{\varphi}^{(1)}(\boldsymbol{X}^{(1)}, t) \in \gamma_c^{(1)}$ as the slave node, which should be prohibited to penetrate the opposing master surface $\Gamma_c^{(2)}$ rather than its spatial counterpart $\gamma_c^{(2)*}$. Using the closest point projection

$$\min \|\boldsymbol{\varphi}^{(1)}(\boldsymbol{X}^{(1)}) - \boldsymbol{\varphi}^{(2)}(\boldsymbol{X}^{(2)})\| \tag{13}$$

we obtain $\boldsymbol{\varphi}^{(2)}(\bar{\boldsymbol{X}}^{(2)}(\boldsymbol{X}^{(1)}))$ with closest distance to the slave node $\boldsymbol{\varphi}^{(1)}(\boldsymbol{X}^{(1)})$. In the following we neglect the arguments of the slave point $\boldsymbol{\varphi}^{(1)} := \boldsymbol{\varphi}^{(1)}(\boldsymbol{X}^{(1)})$ and its corresponding master point $\bar{\boldsymbol{\varphi}}^{(2)} := \boldsymbol{\varphi}^{(2)}(\bar{\boldsymbol{X}}^{(2)}(\boldsymbol{X}^{(1)}))$. The master surface corresponds to a 2-D manifold which we parametrize using convective coordinates ξ^1, ξ^2 (see Figure 2). Therefore the aforementioned master node is characterized by

$$\bar{\boldsymbol{\varphi}}^{(2)} := \boldsymbol{\varphi}^{(2)}(\bar{\xi}^1, \bar{\xi}^2), \quad \boldsymbol{X}^{(2)} := \boldsymbol{X}^{(2)}(\bar{\xi}^1, \bar{\xi}^2) \tag{14}$$

where $\bar{\xi}^1, \bar{\xi}^2$ denote the projection point corresponding to $\bar{\boldsymbol{X}}^{(2)}$. Thus, we are able to define the spatial bases for the projection point moving with the slave point $\boldsymbol{\varphi}^{(1)}$

$$\boldsymbol{a}_j := \boldsymbol{\varphi}^{(2)}_{,\xi^j}(\bar{\xi}^1, \bar{\xi}^2) \tag{15}$$

In this connection we define the gap function

$$g = \boldsymbol{n} \cdot \left(\boldsymbol{\varphi}^{(1)} - \bar{\boldsymbol{\varphi}}^{(2)} \right) \tag{16}$$

where $\boldsymbol{n}$ denotes the unit outward normal to $\gamma_c^{(2)}$ at $\bar{\boldsymbol{\varphi}}^{(2)}$. With the bases for the projection point at hand we introduce the outward unit normal

$$\boldsymbol{n} = \frac{\boldsymbol{a}_1 \times \boldsymbol{a}_2}{\|\boldsymbol{a}_1 \times \boldsymbol{a}_2\|} \tag{17}$$

The contact traction can be subdivided into a normal and a tangential part due to their different physical behaviour in the different directions:

$$\boldsymbol{t} := \boldsymbol{t}^{(1)} = t_N \, \boldsymbol{n} + \boldsymbol{t}_T \tag{18}$$

The normal contact conditions, well-known as the Karush-Kuhn-Tucker conditions, are given by

$$g \geq 0 \tag{19}$$
$$t_N = \boldsymbol{t} \cdot \boldsymbol{n} \leq 0 \tag{20}$$
$$t_N \, g = 0 \tag{21}$$

For frictional contact we further have to incorporate tangential contact conditions in terms of a frictional constitutive law. Here we make use of Coulomb's friction law, for which the tangential contact conditions can be stated as (see Reference [9]):

$$\phi = \|\boldsymbol{t}_T\| - \mu \, t_N \leq 0 \tag{22}$$
$$\boldsymbol{v}_T = -\zeta \, \frac{\boldsymbol{t}_T}{\|\boldsymbol{t}_T\|} \tag{23}$$
$$\zeta \geq 0 \tag{24}$$
$$\zeta \, \phi = 0 \tag{25}$$

where $\boldsymbol{v}_T$ denotes the tangential velocity and ζ denotes the consistency parameter. Finally we obtain the virtual contact work decomposed into the normal and the tangential part via

$$G^c(\boldsymbol{\varphi}, \delta\boldsymbol{\varphi}) = \int_{\Gamma_c^{(1)}} \left[t_N \, \boldsymbol{n} + t_{T_j} \, \boldsymbol{a}^j \right] \cdot \left[\delta\boldsymbol{\varphi}^{(1)} - \delta\bar{\boldsymbol{\varphi}}^{(2)} \right] \, \mathrm{d}A \tag{26}$$

$$= \int_{\Gamma_c^{(1)}} \left(t_N \, \delta g + t_{T_j} \, \delta\bar{\xi}^j \right) \, \mathrm{d}A \tag{27}$$

---

*In the continuous setting the choice whether $\boldsymbol{X}^{(1)}$ or $\boldsymbol{X}^{(2)}$ is defined as slave node is arbitrary.

4 Spatial discretization

For the numerical treatment of the underlying weak form (see Equation (9)) we first accomplish the spatial discretization leading either to a set of ordinary differential equations (ODE's) or DAE's (continuous in time), dependent on the used method for incorporation of the contact constraints. After this we consider the temporal discretization in Section 6. For the spatial discretization we use displacement-based finite elements. Therefore the bodies $\mathcal{B}^{(i)}$ are subdivided into a finite number of elements n_{el}

$$\mathcal{B}^{(i)} \approx \mathcal{B}^{(i),h} = \bigcup_e^{n_{el}} \mathcal{B}_e^{(i),h} \tag{28}$$

where e corresponds to the respective element. For the solution, the test function and the reference configuration, we use the following approximations

$$\boldsymbol{\varphi}^{(i),h} = \sum_{I=1}^{n_{node}} N_I \, \boldsymbol{\varphi}_I^{(i)}, \quad \delta\boldsymbol{\varphi}^{(i),h} = \sum_{J=1}^{n_{node}} N_J \, \delta\boldsymbol{\varphi}_J^{(i)}, \quad \boldsymbol{X}^{(i),h} = \sum_{K=1}^{n_{node}} N_K \, \boldsymbol{X}_K^{(i)} \tag{29}$$

where $\boldsymbol{\varphi}_I^{(i)}$, $\delta\boldsymbol{\varphi}_J^{(i)}$ and $\boldsymbol{X}_K^{(i)}$ denote the nodal counterparts of $\boldsymbol{\varphi}^{(i),h}$, $\delta\boldsymbol{\varphi}^{(i),h}$ and $\boldsymbol{X}^{(i),h}$. In Equation (29) $N_{(\bullet)}$ denote the shape functions for an eight-node tri-linear brick element. Concerning the spatial discretization of the weak form in Equation (10) we obtain the semi-discrete virtual work for both bodies using the approximations in Equation (29) via

$$\sum_{i=1}^{2} \left(\overbrace{\int_{\mathcal{B}^{(i),h}} \rho \, N_I \, N_J \, \mathrm{d}V}^{=:M_{IJ}^{(i)}} \ddot{\boldsymbol{\varphi}}_J^{(i),h} \cdot \delta\boldsymbol{\varphi}^{(i),h} + \overbrace{\int_{\mathcal{B}^{(i),h}} \left(\nabla_{\mathrm{X}^{(i)}} N_I \cdot \boldsymbol{S}^h \right) \cdot \nabla_{\mathrm{X}^{(i)}} N_J \, \mathrm{d}V \, \boldsymbol{\varphi}_J^{(i),h}}^{=:\boldsymbol{f}^{(i),int}} \cdot \delta\boldsymbol{\varphi}^{(i),h} \right.$$

$$\left. \underbrace{- \int_{\mathcal{B}^{(i),h}} N_I \, \rho \, \bar{\boldsymbol{B}}^h \, \mathrm{d}V \cdot \delta\boldsymbol{\varphi}^{(i),h} - \int_{\Gamma_n^{(i),h}} \hat{N}_I \, \bar{\boldsymbol{T}}^h \, \mathrm{d}A \cdot \delta\boldsymbol{\varphi}^{(i),h}}_{=:\boldsymbol{f}_I^{(i),ext}} \right) + G^{c,h} = 0 \tag{30}$$

where $\boldsymbol{S}$ denotes the second Piola-Kirchhoff stress tensor. Consistent with the eight-node brick elements used for the isoparametric discretization of the bodies, the shape functions $\hat{N}_I$ in Equation (30) are bi-linear and restricted to the surface. In Equation (30) the integrals over the domain can be approximated via the sum over all domain elements $e = 1, ..., n_{el}$

$$\int_{\mathcal{B}^{(i),h}} (\bullet) \, \mathrm{d}V \approx \sum_{e=1}^{n_{el}} \int_{\mathcal{B}_e^{(i),h}} (\bullet) \, \mathrm{d}V \tag{31}$$

and the integrals over the Neumann surface can be approximated via the sum over all Neumann boundary elements $n = 1, ..., n_n$

$$\int_{\Gamma_n^{(i),h}} (\bullet) \, \mathrm{d}A \approx \sum_{n=1}^{n_n} \int_{\Gamma_{n,n}^{(i),h}} (\bullet) \, \mathrm{d}A \tag{32}$$

The remaining integrals in Equation (32) on the right hand side can be evaluated using standard quadrature rules. In summary, we obtain the semi-discrete virtual work

$$G^h(\boldsymbol{\varphi}, \delta\boldsymbol{\varphi}) = \sum_{i=1}^{2} \delta\boldsymbol{\varphi}_I^{(i)} \left[M_{IJ}^{(i)} \ddot{\boldsymbol{\varphi}}_J^{(i)} + \boldsymbol{f}_I^{(i),int} + \boldsymbol{f}_I^{(i),ext} \right] + G^{c,h} = 0 \tag{33}$$

where $M_{IJ}^{(i)}$ denotes the nodal mass contribution.

NTS-Element   Similar to the approximations done for the solution, test function and the reference configuration we use the following approximations for the contact boundaries

$$\boldsymbol{\varphi}_c^{(i),h} = \sum_{I}^{n_{node}} \hat{N}_I \, \boldsymbol{\varphi}_I^{(i)}, \quad \delta\boldsymbol{\varphi}_c^{(i),h} = \sum_{J}^{n_{node}} \hat{N}_J \, \delta\boldsymbol{\varphi}_J^{(i)}, \quad \boldsymbol{X}_c^{(i),h} = \sum_{K}^{n_{node}} \hat{N}_K \, \boldsymbol{\varphi}_K^{(i)} \tag{34}$$

where unlike Equation (29) $\hat{N}_{(\bullet)}$ denote bilinear shape functions and n_{node} denotes the number of element nodes. For the description of the virtual contact work we use the well known NTS-method (see for example the textbooks Reference [13, 10]) as depicted in Figure 3. As determined in Section 3, $\boldsymbol{X}^{(1)} \in \Gamma^{(1)}$ is regarded as a slave node with its corresponding master surface $\Gamma^{(2)}$. Concerning the contact virtual work
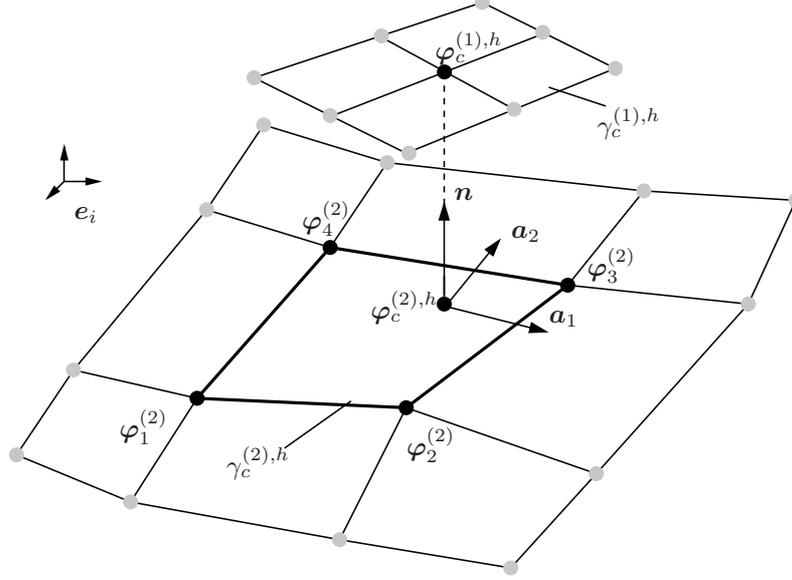
Figure 3. Three-dimensional five node NTS-element.

we only need to consider the solution and test functions corresponding to the contact surface. The discrete gap function g^h can be calculated via

$$g^h = \left(\boldsymbol{\varphi}_c^{(1),h} - \boldsymbol{\varphi}_c^{(2),h} \right) \cdot \boldsymbol{n}^h \tag{35}$$

Accordingly, the discrete virtual contact work reads

$$G^{c,h} = \int_{\Gamma_c^{(1)h}} \left(t_N^h \, \delta g^h + t_{T_j}^h \, \delta\bar{\xi}^{j,h} \right) \, \mathrm{d}A \tag{36}$$

and can be obtained by the sum over all surface elements

$$G^{c,h} = \sum_{s=1}^{n_c} \int_{\Gamma_{e,c}^h} \left(t_{N_s}^h \, \delta g_s^h + t_{T_{js}}^h \, \delta\bar{\xi}_s^{j,h} \right) \, \mathrm{d}A \tag{37}$$

where index notation is used. In Equation (37) $s = 1, ..., n_c$ denotes the s-th contact element and the remaining integrals can be evaluated as usual.

5   Equation of motion

For the incorporation of the contact constraints different methods exists. The most important are the Lagrange multiplier method and the penalty method. The Lagrangian for the constraint system is given by:

$$L_\lambda = \frac{1}{2} \, \dot{\boldsymbol{\varphi}} \cdot \boldsymbol{M} \, \dot{\boldsymbol{\varphi}} - V(\boldsymbol{\varphi}) - \sum_{s=1}^{n_c} \phi_s(\boldsymbol{\varphi}) \, \boldsymbol{\lambda}_s \tag{38}$$

Using Equation (38) we obtain the following semi-discrete index-3 DAE's:

$$M\ddot{\boldsymbol{\varphi}} + \nabla V(\boldsymbol{\varphi}) + \sum_{s=1}^{n_c} \boldsymbol{G}_s^{\mathrm{T}}(\boldsymbol{\varphi})\,\boldsymbol{\lambda}_s = \mathbf{0} \tag{39}$$

$$\begin{bmatrix} \phi_1 \\ \vdots \\ \phi_{n_c} \end{bmatrix} = \mathbf{0} \tag{40}$$

Here $\boldsymbol{G}_s$ denotes the gradient of the constraints ϕ with respect to the configuration. For the penalty method we obtain ordinary differential equations instead of DAE's. But in the following we focus on the Lagrange multiplier method.

5.1 Frictionless contact

For the frictionless case, each contact element incorporates the constraint

$$\phi_s^N = g_s$$

with its corresponding Lagrange multiplier λ_{N_s}. We obtain the DAE's

$$M\ddot{\boldsymbol{\varphi}} + \nabla V(\boldsymbol{\varphi}) + \sum_{s=1}^{n_c} \boldsymbol{G}_s^{N,\mathrm{T}}(\boldsymbol{\varphi})\,\lambda_{N_s} = \mathbf{0} \tag{41}$$

$$\begin{bmatrix} \phi_1^N \\ \vdots \\ \phi_{n_c}^N \end{bmatrix} = \mathbf{0} \tag{42}$$

Standard integrators like e.g. the midpoint-rule or the Newmark-scheme applied for the time discretization of the DAE's (41-42) fail to consistently reproduce the total energy of the system leading to an unstable numerical behaviour of the system. Therefore we propose in the following a mixed approach together with the concept of a discrete gradient leading to an energy and momentum consistent integration scheme.

Mixed approach As mentioned above we apply an energy-momentum scheme proposed in References [6, 3] for frictionless contact. In order to design such an energy-momentum scheme we introduce additional coordinates $\boldsymbol{d}_s \in \mathbb{R}^3$ and the vector $\boldsymbol{f}_s \in \mathbb{R}^3$ which corresponds to the normal $\boldsymbol{n}$ and to the convective coordinates $\boldsymbol{\xi}$ respectively. To determine the augmented coordinates we introduce augmented constraints ϕ_s^{aug} to link the new coordinates to the actual configuration. Together with the NTS-constraint ϕ_s^N we obtain:

$$\boldsymbol{g}_s(\boldsymbol{\varphi}_s, \boldsymbol{d}_s, \boldsymbol{f}_s) = \begin{bmatrix} \phi_s^N \\ \phi_s^{aug} \end{bmatrix} \tag{43}$$

For more details about the fundamental properties of this formulation we refer to Reference [6]. With regard to Cauchy's representation theorem, Equation (38) can be reparametrized by using at most quadratic invariants $\boldsymbol{\pi}$. One obtains an augmented Lagrangian of the considered system:

$$\tilde{L}_\lambda = \frac{1}{2}\,\dot{\boldsymbol{\varphi}} \cdot M\,\dot{\boldsymbol{\varphi}} - V(\boldsymbol{\varphi}) - \sum_{s=1}^{n_c} \tilde{\boldsymbol{g}}_s(\boldsymbol{\pi}(\boldsymbol{\varphi}_s, \boldsymbol{d}_s, \boldsymbol{f}_s)) \cdot \boldsymbol{\lambda}_s \tag{44}$$

We define seventeen appropriate invariants (see References [6, 3])

$$\boldsymbol{\pi}(\boldsymbol{\varphi}_s, \boldsymbol{d}_s, \boldsymbol{f}_s) = \begin{bmatrix} \pi_1 \\ \vdots \\ \pi_{17} \end{bmatrix} \tag{45}$$

in order to reformulate the constraints $\tilde{\boldsymbol{g}}_s\left(\boldsymbol{\pi}\left(\boldsymbol{\varphi}_s, \boldsymbol{d}_s, \boldsymbol{f}_s\right)\right)$. The semi-discrete equations of motion can be obtained by the Lagrangian and we finally arrive at:

$$\boldsymbol{M}\,\ddot{\boldsymbol{\varphi}} + \nabla V(\boldsymbol{\varphi}) + \sum_{s=1}^{n_c}\left(\mathrm{D}_1\,\boldsymbol{\pi}(\boldsymbol{\varphi}_s, \boldsymbol{d}_s, \boldsymbol{f}_s)\right)^{\mathrm{T}}\,\nabla_{\boldsymbol{\pi}}\tilde{\boldsymbol{g}}_s(\boldsymbol{\pi})\cdot\boldsymbol{\lambda}_s = \boldsymbol{0} \tag{46}$$

$$\sum_{s=1}^{n_c}\left(\mathrm{D}_2\,\boldsymbol{\pi}(\boldsymbol{\varphi}_s, \boldsymbol{d}_s, \boldsymbol{f}_s)\right)^{\mathrm{T}}\,\nabla_{\boldsymbol{\pi}}\tilde{\boldsymbol{g}}_s(\boldsymbol{\pi})\cdot\boldsymbol{\lambda}_s = \boldsymbol{0} \tag{47}$$

$$\sum_{s=1}^{n_c}\left(\mathrm{D}_3\,\boldsymbol{\pi}(\boldsymbol{\varphi}_s, \boldsymbol{d}_s, \boldsymbol{f}_s)\right)^{\mathrm{T}}\,\nabla_{\boldsymbol{\pi}}\tilde{\boldsymbol{g}}_s(\boldsymbol{\pi})\cdot\boldsymbol{\lambda}_s = \boldsymbol{0} \tag{48}$$

$$\begin{bmatrix}\tilde{\boldsymbol{g}}_1(\boldsymbol{\pi}(\boldsymbol{\varphi}_1, \boldsymbol{d}_1, \boldsymbol{f}_1)) \\ \vdots \\ \tilde{\boldsymbol{g}}_{n_c}(\boldsymbol{\pi}(\boldsymbol{\varphi}_{n_c}, \boldsymbol{d}_{n_c}, \boldsymbol{f}_{n_c}))\end{bmatrix} = \boldsymbol{0} \tag{49}$$

Again we refer to Reference [6] for the derivation of the fundamental properties of the constraints and for the verification of the conservation of the angular momentum $\boldsymbol{J} = \sum_{I,J} M_{I,J}\,\boldsymbol{\varphi}_I \times \dot{\boldsymbol{\varphi}}_J$ as well as of the total energy $E(\boldsymbol{\varphi}, \dot{\boldsymbol{\varphi}}) = \frac{1}{2}\,\dot{\boldsymbol{\varphi}}\cdot\boldsymbol{M}\,\dot{\boldsymbol{\varphi}} + V(\boldsymbol{\varphi})$ of the semi-discrete system.

5.2   Frictional contact

For frictional contact we have to distinguish whether stick or slip occurs. To this end usually a return mapping scheme (for more details see References [10, 13]) is implemented that works as follows. One first assumes stick and computes therefore a trial state ($\boldsymbol{\lambda}_T^{trial}$) during the increment. Then the slip condition can be evaluated:

$$\Psi_{n+1}^{trial} = \|\boldsymbol{\lambda}_{T,n+1}^{trial}\| - \mu\,\lambda_{N,n+1} \tag{50}$$

where μ denotes the coefficient of friction. Stick occurs if $\Psi_{n+1}^{trial} \leq 0$ and else slip occurs. In this connection the frictional tractions $\lambda_{Tj,n+1}$ will be determined

$$\lambda_{Tj,n+1} = \begin{cases}\lambda_{Tj,n+1}^{trial} & \text{if } \Psi_{n+1}^{trial} \leq 0 \quad\text{(stick)} \\ -\mu\,\lambda_{N,n+1}\,\dfrac{\lambda_{Tj,n+1}^{trial}}{\|\boldsymbol{\lambda}_{T,n+1}^{trial}\|} & \text{if } \Psi_{n+1}^{trial} > 0 \quad\text{(slip)}\end{cases} \tag{51}$$

Thus, for the stick case we have to incorporate the constraints

$$\boldsymbol{\phi}_s = \begin{bmatrix}\phi_s^N \\ \phi_s^{T1} \\ \phi_s^{T2}\end{bmatrix} \tag{52}$$

corresponding to the Lagrange multipliers λ_N, λ_{T1} and λ_{T2}. We obtain the DAE's

$$\boldsymbol{M}\,\ddot{\boldsymbol{\varphi}} + \nabla V(\boldsymbol{\varphi}) + \sum_{s=1}^{n_c}\boldsymbol{G}_s^{stick,\mathrm{T}}(\boldsymbol{\varphi})\,\boldsymbol{\lambda}_s = \boldsymbol{0} \tag{53}$$

$$\begin{bmatrix}\boldsymbol{\phi}_1 \\ \vdots \\ \boldsymbol{\phi}_{n_c}\end{bmatrix} = \boldsymbol{0} \tag{54}$$

In case of slip we have to incorporate only the constraint for the normal part

$$\boldsymbol{\phi}_s = \phi_s^N \tag{55}$$

corresponding to the Lagrange multiplier λ_N. The frictional tractions $\lambda_{Tj,n+1}$ for slip are not independent Lagrange multipliers (see Reference [14]) and will be calculated according to Equation (51)$_2$. Finally we

obtain the DAE's

$$M\ddot{\boldsymbol{\varphi}} + \nabla V(\boldsymbol{\varphi}) + \sum_{s=1}^{n_c} \boldsymbol{G}_s^{slip,\mathrm{T}}(\boldsymbol{\varphi})\,\boldsymbol{\lambda}_s = \boldsymbol{0} \tag{56}$$

$$\begin{bmatrix} \phi_1^N \\ \vdots \\ \phi_{n_c}^N \end{bmatrix} = \boldsymbol{0} \tag{57}$$

6 Time discretization

For the time discretization we divide the time interval $\mathcal{I} = [0, T] = \bigcup_{n=0}^{N-1} [t_n, t_{n+1}]$ into equidistant increments $h = t_{n+1} - t_n$ to apply an one step time integration scheme. In the following the time discretization of both the frictionless and frictional contact problems will be considered. For later comparison we apply a standard midpoint rule and a newly developed energy-momentum scheme (firstly presented in Reference [6]) in order to investigate the numerical properties of the latter.

6.1 Midpoint rule

For the midpoint rule the configuration and velocity are evaluated in the midpoint, thus we finally obtain the discrete equations:

$$\boldsymbol{\varphi}_{n+1} - \boldsymbol{\varphi}_n - h\,\boldsymbol{v}_{n+\frac{1}{2}} = \boldsymbol{0} \tag{58}$$

$$\boldsymbol{M}\,(\boldsymbol{v}_{n+1} - \boldsymbol{v}_n) + h\left(\nabla V(\boldsymbol{\varphi}_{n+\frac{1}{2}}) + \sum_{s=1}^{n_c} \boldsymbol{G}_s^{\mathrm{T}}(\boldsymbol{\varphi}_{n+\frac{1}{2}})\,\boldsymbol{\lambda}_{s,n+1}\right) = \boldsymbol{0} \tag{59}$$

$$\begin{bmatrix} \phi_{1,n+1} \\ \vdots \\ \phi_{n_c,n+1} \end{bmatrix} = \boldsymbol{0} \tag{60}$$

This algebraic system of nonlinear equations will be solved by applying Newton's method.

6.2 Energy-momentum scheme - mixed formulation

We aim at the time discretization using a mixed formulation (see Section 5.1), where the NTS constraints are reformulated in appropriate invariants. The next step to design an energy-momentum scheme is to apply a discrete gradient in the sense of Gonzalez (see References [6, 4]). This creates an energy-momentum scheme which besides the algorithmic consistency of both momentum maps is able to conserve the total energy of the system. Finally we can write the completely discrete system within the concept of the discrete gradient as follows:

$$\boldsymbol{\varphi}_{n+1} - \boldsymbol{\varphi}_n - h\,\boldsymbol{v}_{n+\frac{1}{2}} = \boldsymbol{0} \tag{61}$$

$$\boldsymbol{M}\,(\boldsymbol{v}_{n+1} - \boldsymbol{v}_n) + h\,\overline{\nabla}_{\boldsymbol{\varphi}}\,V(\boldsymbol{\varphi}_n, \boldsymbol{\varphi}_{n+1}) \tag{62}$$

$$+h\sum_{s=1}^{n_c}\left(\mathrm{D}_1\,\boldsymbol{\pi}(\boldsymbol{\varphi}_{s,n+\frac{1}{2}}, \boldsymbol{d}_{s,n+\frac{1}{2}}, \boldsymbol{f}_{s,n+\frac{1}{2}})\right)^{\mathrm{T}} \overline{\overline{\nabla}}_{\boldsymbol{\pi}}\,\tilde{\boldsymbol{g}}_s(\boldsymbol{\pi}_n, \boldsymbol{\pi}_{n+1}) \cdot \boldsymbol{\lambda}_{s,n+1} = \boldsymbol{0} \tag{63}$$

$$\sum_{s=1}^{n_c}\left(\mathrm{D}_2\,\boldsymbol{\pi}(\boldsymbol{\varphi}_{s,n+\frac{1}{2}}, \boldsymbol{d}_{s,n+\frac{1}{2}}, \boldsymbol{f}_{s,n+\frac{1}{2}})\right)^{\mathrm{T}} \overline{\overline{\nabla}}_{\boldsymbol{\pi}}\,\tilde{\boldsymbol{g}}_s(\boldsymbol{\pi}_n, \boldsymbol{\pi}_{n+1}) \cdot \boldsymbol{\lambda}_{s,n+1} = \boldsymbol{0} \tag{64}$$

$$\sum_{s=1}^{n_c}\left(\mathrm{D}_3\,\boldsymbol{\pi}(\boldsymbol{\varphi}_{s,n+\frac{1}{2}}, \boldsymbol{d}_{s,n+\frac{1}{2}}, \boldsymbol{f}_{s,n+\frac{1}{2}})\right)^{\mathrm{T}} \overline{\overline{\nabla}}_{\boldsymbol{\pi}}\,\tilde{\boldsymbol{g}}_s(\boldsymbol{\pi}_n, \boldsymbol{\pi}_{n+1}) \cdot \boldsymbol{\lambda}_{s,n+1} = \boldsymbol{0} \tag{65}$$

$$\begin{bmatrix} \tilde{\boldsymbol{g}}_1(\boldsymbol{\pi}(\boldsymbol{\varphi}_{1,n+1}, \boldsymbol{d}_{1,n+1}, \boldsymbol{f}_{1,n+1})) \\ \vdots \\ \tilde{\boldsymbol{g}}_{n_c}(\boldsymbol{\pi}(\boldsymbol{\varphi}_{n_c,n+\frac{1}{2}}, \boldsymbol{d}_{n_c,n+\frac{1}{2}}, \boldsymbol{f}_{n_c,n+\frac{1}{2}})) \end{bmatrix} = \boldsymbol{0} \tag{66}$$

Here the discrete gradient $\overline{\nabla}_{\varphi} \, V(\varphi_n, \varphi_{n+1})$ applied to the internal energy is used (for more details see Reference [2]). In addition, the discrete gradient $\overline{\overline{\nabla}}_{\pi} \, \tilde{g}(\pi_n, \pi_{n+1})$ is defined as follows:

$$\overline{\overline{\nabla}}_{\pi} \, \tilde{g}_s(\pi_n, \pi_{n+1}) = \nabla_{\pi} \, \tilde{g}_s \left(\pi_{n+\frac{1}{2}} \right)$$

$$+ \frac{\tilde{g}_s(\pi_{n+1}) - \tilde{g}_s(\pi_n) + \nabla_{\pi} \, \tilde{g}_s \left(\pi_{n+\frac{1}{2}} \right) (\pi_{s,n+1} - \pi_{s,n})}{\|\pi_{s,n+1} - \pi_{s,n}\|^2} \, (\pi_{s,n+1} - \pi_{s,n}) \qquad (67)$$

The verification of the conservation of the angular momentum and the total energy of the discrete system can be found in Reference [6]. In this connection we have to remark that the consistency condition is violated in general by an inactive constraint, which gets active within a specific time step. Further details can be found in References [3, 6].

REFERENCES

[1]   Armero, F.; and Petöcz, E.; Formulation and analysis of conserving algorithms for frictionless dynamic contact/impact problems. Comput. Methods Appl. Mech. Engrg., Vol. 158, pp. 269–300, 1998.

[2]   Betsch, P.; Steinmann, P.; Conservation properties of a time FE method. Part III: Mechanical systems with holonomic constraints. Int. J. Numer. Meth. Engng, Vol. 53, pp. 2271–2304, 2002.

[3]   Franke, M.; Hesch C.; Betsch P.; Energy-momentum consistent integration of frictional multibody contact problems. In Proceedings of the ECCOMAS Thematic Conference, Brussels, 2011.

[4]   Gonzalez, O.; Time integration and discrete Hamiltonian systems. Journal of Nonlinear Science, Vol. 6, pp. 449–467, 1996.

[5]   Hallquist, J.O.; NIKE2D: An implicit, finite-deformation, finite-element code for analyzing the static and dynamic response of two-dimensional solids. Technical Report UCRL-52678, Lawrence Livermore Laboratory, Livermore, CA, 1979.

[6]   Hesch, C.; Betsch, P.; Transient 3d contact problems – NTS method: Mixed methods and conserving integration. Computational Mechanics, Vol. 48, pp. 437–449, 2011.

[7]   Holzapfel, G.A.; Nonlinear solid mechanics. John Wiley & Sons, 2000.

[8]   Konyukhov, A.; Schweizerhof, K.; Covariant description for frictional contact problems. Computational Mechanics, DOI: 10.1007/s00466-004-0616-7, Springer-Verlag, 2004.

[9]   Laursen, T.A.; Simo J.C.; A continuum-based finite element formulation for the implicit solution of multibody, large deformation frictional contact problems. Int. J. Numer. Meth. Engng, Vol. 36, pp. 3451–3485, 1993.

[10] Laursen, T.A.; Computational contact and impact mechanics. Springer-Verlag, 2002.

[11] Sänger, N.; Elemente für die Dynamik flexibler Mehrkörpersysteme. Ph.D. Thesis, Department of Mechanical Engineering, University of Siegen, 2011.

[12] Uhlar, S.; Energy consistent time-integration of hybrid multibody systems. Ph.D. Thesis, Department of Mechanical Engineering, University of Siegen, 2009.

[13] Wriggers, P.; Computational contact mechanics. Springer-Verlag, 2nd edition, 2006.

[14] Zienkiewicz, O.C.; Taylor, R.L.; The Finite Element Method. For Solid and Structural Mechanics. Butterworth Heinemann, 2005.